Journal of Theoretical Biology 489 (2020) 110158

Contents lists available at ScienceDirect

Journal of Theoretical Biology

journal homepage: www.elsevier.com/locate/jtb

Separate seasons of infection and reproduction can lead to multi-year population cycles

F.M. Hilker[a,*], T.A. Sun[a], L.J.S. Allen[b], F.M. Hamelin[c]

[a] Institute of Environmental Systems Research and Institute of Mathematics, Osnabrück University, D–49069 Osnabrück, Germany
[b] Department of Mathematics and Statistics, Texas Tech University, Lubbock, TX 79409, USA
[c] Agrocampus Ouest, INRAE, Université de Rennes, IGEPP, Rennes, France

ARTICLE INFO

Article history:
Received 5 September 2019
Revised 3 January 2020
Accepted 7 January 2020
Available online 10 January 2020

Keywords:
Host–pathogen dynamics
Pathogen-driven outbreak
Quasi-periodic oscillation
Neimark-Sacker bifurcation
SI model
Difference equations
Seasonal population dynamics

ABSTRACT

Many host–pathogen systems are characterized by a temporal order of disease transmission and host reproduction. For example, this can be due to pathogens infecting certain life cycle stages of insect hosts; transmission occurring during the aggregation of migratory birds; or plant diseases spreading between planting seasons. We develop a simple discrete-time epidemic model with density-dependent transmission and disease affecting host fecundity and survival. The model shows sustained multi-annual cycles in host population abundance and disease prevalence, both in the presence and absence of density dependence in host reproduction, for large horizontal transmissibility, imperfect vertical transmission, high virulence, and high reproductive capability. The multi-annual cycles emerge as invariant curves in a Neimark–Sacker bifurcation. They are caused by a carry-over effect, because the reproductive fitness of an individual can be reduced by virulent effects due to infection in an earlier season. As the infection process is density-dependent but shows an effect only in a later season, this produces delayed density dependence typical for second-order oscillations. The temporal separation between the infection and reproduction season is crucial in driving the cycles; if these processes occur simultaneously as in differential equation models, there are no sustained oscillations. Our model highlights the destabilizing effects of inter-seasonal feedbacks and is one of the simplest epidemic models that can generate population cycles.

1. Introduction

How infectious diseases spread in populations is determined by complex interactions between pathogens, hosts, and their environment. Many host-pathogen systems are characterized by a temporal order of events in which the transmission period of the pathogen is separated from the reproduction period of the host. Such a sequence of infection and breeding periods is a notorious feature of a number of plant and animal populations, especially in the presence of discrete life cycle stages, spatial migration, breeding behavior, or seasonal changes in social mixing, flocking or crowding, and anthropogenic impacts.

For example, many defoliating insects have certain stage classes, where only larvae or pupae can become parasitized (Volkman, 1997; Cory and Myers, 2003; Miller, 2013). Agricultural crops have clearly defined planting periods, after which diseases may be transmitted by insect vectors (Mailleret and Lemesle, 2009). In migratory species, breeding in summer is often followed by an autumnal aggregation period before starting the long-distance movements (Dingle, 1996). During the aggregation period, there is notable variation in parasite pressure for insects, birds, and mammals (Folstad et al., 1991; Loehle, 1995; Altizer et al., 2011). Avian influenza incidence has been suggested to peak in migratory waterfowl in late summer and early fall, whereas there is little infection in winter (Hinshaw et al., 1980; Krauss et al., 2004; Munster et al., 2007; Hoye et al., 2011). Another kind of aggregation can occur at bird feeders in fall and winter, where the flocking behavior has been suggested to increase the transmission and prevalence of *Mycoplasma gallisepticum* in house finches (Altizer et al., 2004; Hosseini et al., 2004).

Breeding behavior can also play a crucial role in driving pathogen transmission. European red foxes (*Vulpes vulpes*) show increased mobility during the mating season, which leads to increased transmission of rabies, while parents become more sedentary when raising their offspring and are thus less likely to transmit the disease (Pastoret and Brochier, 1999; Bolzoni et al., 2008). Aggressive interactions (between males) or courtship-related contacts during the breeding season could be further mechanisms

* Corresponding author.
E-mail address: frank.hilker@uni-osnabrueck.de (F.M. Hilker).

https://doi.org/10.1016/j.jtbi.2020.110158
0022-5193/

driving seasonal transmission of pathogens (Keeling and Rohani, 2007).

Hence, there is ample evidence that disease transmission occurs predominantly or is amplified in certain seasons of the year. Mathematical models are useful tools for investigating the dynamic interplay between the processes in the different seasons. Previous models have used alternative frameworks to investigate separate seasons of infection and reproduction, including difference equations (Régnière, 1984; Hamelin et al., 2017), semi-discrete or hybrid systems (van den Berg et al., 2011; Hamelin et al., 2011; 2016a; 2016b; Mailleret et al., 2012; Hilker et al., 2017; Desprez-Loustau et al., 2019), and delay differential equations (Briggs and Godfray, 1995a; 1995b; 1996).

Here we use difference equations because they are easier to analyze and particularly appropriate when there are non-overlapping seasons with distinct transmission and reproduction processes. Our model is similar to the one in Hamelin et al. (2017), with the only difference that we assume density-dependent rather than frequency-dependent transmission. The former is often more appropriate for directly or environmentally transmitted pathogens, while the latter is often more appropriate for sexually or vector transmitted pathogens (cf. Begon et al., 2002). Our model is also similar to the one in Régnière (1984), but differs from it by adding density-dependent host population regulation and ignoring nonlinear transmission functions as well as different disease states.

In this paper, we show that separate seasons of disease transmission and host reproduction can drive multi-year cycles of both the host population and the disease prevalence, provided that disease transmission is density-dependent and the disease sufficiently virulent. We offer an explanation of the mechanisms causing these cycles. The important point is that the infection status of an individual, obtained in one season of the year, affects the fitness of the same individual during breeding in another season of the year. This results in a carry-over effect (Norris, 2005), which is destabilizing in this case. Hence, the cycle mechanism is clearly different from other causes like seasonal variation or external forcing, which have been reviewed by Altizer et al. (2006). Also, discrete-time models can be constructed in different ways. One commonly taken approach is to numerically discretize differential equation models. However, that can lead to oscillations and chaos even in the absence of disease, e.g. when logistic host population growth is approximated by the discrete quadratic map. Here, we use instead an "exponential approach" based on the Poisson distribution that can be traced back to Reed and Frost. This implies that the multi-annual oscillations are not due to numerical discretization, but an emergent system property.

In the next section, we derive the mathematical model. Numerical simulations of its dynamical behavior including discrete-time limit cycles will be shown in the following section, while the equilibrium and stability analysis is available in the Appendix. In the Discussion, we compare our model dynamics with empirical examples that show some qualitative agreement. We also discuss the mechanism driving the oscillations and point out the differences with other epidemiological models that generate population cycles.

2. Model

We formulate a discrete-time model of a host population, where the time step corresponds to one generation (life cycle length). Without loss of generality, we assume that the completion of the life cycle takes one year, and we will use the terms generation, time step, and year interchangeably in this paper. Each generation is composed of two temporally distinct periods (seasons): (i) horizontal transmission, denoted by Infection; (ii) reproduction, competition, survival, and vertical transmission, denoted by Reproduction.

In the main text, we assume that Reproduction occurs after Infection:

$$t \underbrace{\rightarrow}_{\text{Infection}} t' \underbrace{\rightarrow}_{\text{Reproduction}} t+1\,.$$

During the time interval $[t, t']$, horizontal disease transmission between infected and susceptible hosts occurs. During this first time interval, an epidemic may occur. During the second time interval $[t', t+1]$, hosts reproduce and die. Vertical disease transmission between an infected host and its progeny can also occur during this second time interval. After the second period, the annual cycle repeats.

Appendix A shows that the order of events (whether Reproduction occurs before Infection or the other way around) does not impact the main result to be presented (multi-year cycles may occur in a simple discrete-time epidemic model).

Two variables account for the host population dynamics during each of the periods. The two variables are S and I, the density of susceptible and infected hosts, respectively. The total density of susceptible and infected hosts is denoted as $N = S + I$. The host dynamics are observed each year before Infection at time t, $t = 0, 1, 2, \ldots$.

During the Infection period, the Poisson distribution is used to model horizontal disease transmission between the infected and susceptible hosts. We assume that transmission is density-dependent. Let Λ denote the parameter in the Poisson distribution. Then $\Lambda = \beta I$ is the average number of contacts with infected hosts over an Infection season that result in horizontal disease transmission to one susceptible host. Hence, the probability of no successful disease transmission to the susceptible host is $\exp(-\Lambda)$ and the probability of successful transmission is $1 - \exp(-\Lambda)$. Therefore, at time t', the model takes the form:

$$\begin{aligned} S(t') &= S(t)\exp\left(-\beta I(t)\right), \\ I(t') &= I(t) + S(t)[1 - \exp\left(-\beta I(t)\right)]. \end{aligned} \tag{1}$$

We would like to remark that system (1) is formally related to the Reed–Frost model (see Appendix B).

For the Reproduction period, we use a well-known form of compensatory population growth that corresponds to the logistic growth model and goes back to Beverton and Holt (1957) for animal populations and to de Witt (1960) for plants. At time $t+1$, the model is:

$$\begin{aligned} S(t+1) &= \rho_S S(t') + \frac{b_S S(t') + (1-p) b_I I(t')}{1 + \lambda N(t')}, \\ I(t+1) &= \rho_I I(t') + \frac{p b_I I(t')}{1 + \lambda N(t')}, \end{aligned} \tag{2}$$

where ρ_S and ρ_I are the survival fractions of susceptible and infected hosts after giving birth, respectively. The fecundity parameters b_S and b_I denote the average number of viable offspring produced per susceptible or infected host, respectively, in the absence of density-dependent effects. Parameter $\lambda > 0$ describes density-dependent competition between hosts. We assume that density dependence applies equally to susceptible and infected hosts. Our model includes two types of disease transmission. Besides horizontal transmission in the Infection period, there is vertical transmission during the Reproduction period. Parameter $p \in [0, 1]$ accounts for vertical transmission. If there is perfect vertical transmission ($p = 1$), all the offspring produced by an infected host are infected. In the case of imperfect vertical transmission ($0 \leq p < 1$), only a proportion p of the offspring of infected hosts is infected, and the remaining proportion $1 - p$ is not infected.

In the remainder of the paper, we assume that a susceptible host produces on average more than one viable offspring so that susceptible hosts survive in the absence of infection. Moreover, we

Table 1
Model parameters and variables.

Variable	Definition	Parameter	Definition
t	time in years	b_S	susceptible host fecundity
$N(t)$	total host density	b_I	infected host fecundity
$S(t)$	susceptible density	p	vertical transmission fraction
$I(t)$	infected density	β	horizontal transmission rate

assume that infected hosts have lower reproductive output than susceptible hosts. This could be due to disease-reduced fertility or disease-reduced survival of the infected offspring. These assumptions imply:

$$0 < b_I < b_S\,, \quad \text{and} \quad b_S > 1\,.$$

For simplicity, we henceforth also assume that adult individuals die after giving birth, i.e., $\rho_S = \rho_I = 0$, which amounts to focusing on semelparous species (including annual plants). The model simplifies to:

$$S(t+1) = \frac{b_S S(t') + (1-p)b_I I(t')}{1+\lambda N(t')},$$
$$I(t+1) = \frac{pb_I I(t')}{1+\lambda N(t')}. \tag{3}$$

The full model consists of the preceding models for the two periods of Infection and Reproduction. That is, combining Eqs. (1) and (3), the full model can be expressed as the following system of two first-order difference equations for susceptible and infected hosts:

$$S(t+1) = \frac{(1-p)b_I[I(t)+S(t)] + [b_S - (1-p)b_I]S(t)\mathrm{e}^{-\beta I(t)}}{1+\lambda[I(t)+S(t)]},$$
$$I(t+1) = pb_I \frac{I(t)+S(t)\left[1-\mathrm{e}^{-\beta I(t)}\right]}{1+\lambda[I(t)+S(t)]}, \tag{4}$$

with $b_S > 1$, $b_I < b_S$ and $0 < p \le 1$. Table 1 lists the parameters, variables and their definitions for the full model.

Model (4) corresponds to the one in Hamelin et al. (2017), except that it is based on density-dependent rather than frequency-dependent transmission. Moreover, model (4) is related to the one in Régnière (1984), but extends it by density-dependent host demographics and simplifies it by ignoring nonlinear transmission rates due to propagule aggregations and different disease states (see Appendix C for details).

3. Results

Simulations show the existence of sustained oscillations in the host–pathogen model (4), both in the absence and presence of density-dependent reproduction. For $\lambda = 0$, the time series in Fig. 1 shows an example of a large-amplitude multi-year cycle of the total host population density and the disease prevalence, i.e., the proportion of the host population being infected. The two variables oscillate with the same period. Their oscillations are phase-shifted, with the disease prevalence lagging behind the total host density.

3.1. Density-independent reproduction ($\lambda = 0$)

Here, we study more closely the properties of the cycles and the mechanisms causing them, assuming $\lambda = 0$. In the phase plane, the cycle orbit asymptotically forms a closed invariant curve (see Fig. 2). It can be considered a discrete-time limit cycle. The orbit jumps around the closed invariant curve, but never repeats a sequence exactly. Thus it eventually fills out the entire invariant curve. The dynamics on the closed invariant curve are quasi-periodic. In contrast to continuous-time limit cycles, the orbit does not move smoothly around the closed invariant curve.

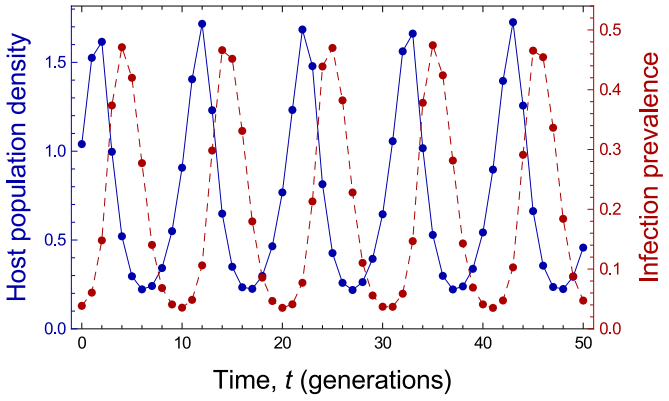

Fig. 1. Time series of total host population abundance $N = S + I$ (blue, solid) and disease prevalence I/N (red, dashed). Obtained from model (4) with $b_S = 2, b_I = 0.5, \beta = 10, p = 0.5, \lambda = 0$. (For interpretation of the references to color in this figure legend, the reader is referred to the web version of this article.)

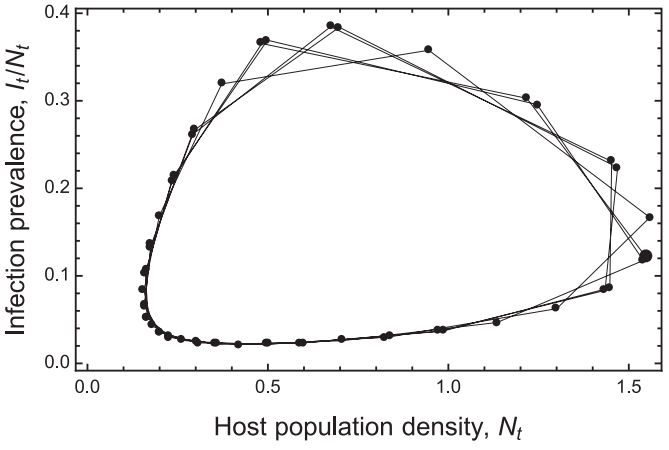

Fig. 2. Invariant curve (discrete-time limit cycle) in the state space of total host population abundance and disease prevalence. Shown are 50 iterations obtained from model (4) with $b_S = 2, b_I = 0.5, \beta = 10, p = 0.5, \lambda = 0$.

Fig. 3 shows a phase plot of total host density N_{t+1} against the lagged density N_t. It reveals a circular clockwise orbit, which indicates that the host population is regulated by delayed density-dependent mechanisms (second-order feedbacks; see Turchin, 2003). In addition, the orbit in Fig. 3 is color-coded to show the disease prevalence. The phase plot may be more easily interpreted when realizing that the orbit follows the total population density, which can be written as

$$N(t+1) = b_I N(t) + (b_S - b_I)\mathrm{e}^{-\beta N(t) z(t)} N(t)(1 - z(t)),$$

where $z(t) = I(t)/N(t) \in [0, 1]$ is the disease prevalence.

Fig. 3 suggests that the multi-year cycle is driven by alternating episodes of host population growth and host population decline. If the disease prevalence is small, the host population consists mostly of susceptible individuals and grows with an overall factor that is close to b_S (where the upper part of the circular orbit is close to the upper dotted line). By contrast, if the disease prevalence is large, the host population consists of so many infected individuals that the overall growth factor is close to b_I (where the lower part of the circular orbit is close to the lower dotted line). The population density then declines because $b_I < 1$ due to virulent effects. When the population density becomes smaller, disease transmission gets reduced as well because it is density-dependent. As a consequence, the disease prevalence decreases and the proportion of susceptibles in the population increases. The overall growth factor therefore again approaches b_S, which allows the host population to enter another growth episode of the cycle.

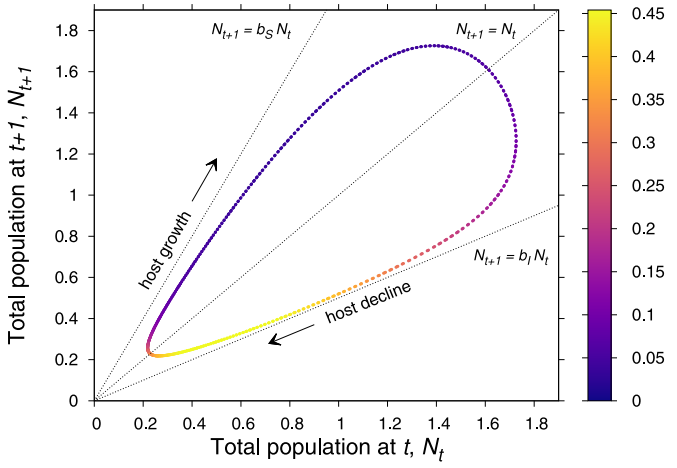

Fig. 3. Phases of host population growth and decline. Color coding according to disease prevalence. The last 1,000 of 5,000 iterations of model (4) are plotted. Parameters: $b_S = 2, b_I = 0.5, \beta = 10, p = 0.5, \lambda = 0$. (For interpretation of the references to color in this figure legend, the reader is referred to the web version of this article.)

Note that, in the examples shown thus far with $\lambda = 0$, the disease regulates a host population that would grow without bounds in the absence of disease to sustained oscillations (cf. Appendix D). The oscillations also occur in the presence of bounded host population growth ($\lambda > 0$). In this case, the dotted lines in Fig. 3 correspond to saturating Beverton–Holt curves (not shown here).

3.2. Density-dependent reproduction ($\lambda > 0$)

Simulations of model (4) with $\lambda > 0$ show that the host–pathogen system converges in the long-term toward either a stable equilibrium or sustained oscillations. We do not observe bistability. The stable equilibrium can be (i) the disease-free equilibrium ($S^* = (b_S - 1)/\lambda, I^* = 0$), where the infected population goes extinct; (ii) a coexistence equilibrium ($S^* > 0$, $I^* > 0$), where both uninfected and infected hosts remain in the long run; or (iii) the total-infection equilibrium ($S^* = 0, I^* = (b_I - 1)/\lambda$), if there is perfect vertical transmission ($p = 1$). Details of the equilibria and their stability are given in Appendix D.

Fig. 4 shows bifurcation diagrams for varying horizontal transmission parameter β. For low values of β, the disease cannot establish in the host population and the disease-free equilibrium is the attractor (see Appendix D for the analytical condition). For intermediate values of β, the disease can invade and persist so that the coexistence equilibrium is the attractor. At a critical value β_{NS}, we observe a Neimark–Sacker bifurcation where the coexistence equilibrium loses stability, giving rise to oscillations for $\beta > \beta_{NS}$. The oscillations can be quasi-periodic like on the closed invariant curve shown in Fig. 2, or they can be periodic cycles. The latter occur in the periodic windows of the bifurcations diagrams in Fig. 4B–D; they are still multi-year oscillations. Periodic cycles are promoted by increased fecundity of susceptible individuals (higher b_S) and by increased virulence (lower b_I). The parameter range of oscillations, quasi-periodic or periodic, increases with both b_S and b_I in Fig. 4. We did not observe chaotic dynamics in our simulations but we did not search for it either.

Fig. 5 is a two-parameter bifurcation diagram. The graph illustrates how the infected host fecundity b_I effectively influences the critical horizontal transmission parameter β_{NS} at which the Neimark–Sacker bifurcation occurs. Our simulations suggest that when b_I is close to 0 or 1, the coexistence equilibrium retains its stability for a larger range of horizontal transmission parameter values than for intermediate values of infected host fecundity.

Now, we investigate the impact of the two remaining parameters λ and p on the population and disease dynamics. First, density dependence ($\lambda > 0$) facilitates the existence of a stable disease-free equilibrium (Fig. 6). That is, while the disease is endemic for $\lambda = 0$ (at stable equilibrium or in form of cycles), the disease dies out in host populations with density-dependent demographics if horizontal transmission and infected host fecundity are small. Moreover, increased density dependence (larger values of λ) is stabilizing in the sense of reducing the parameter range leading to endemic cycles (compare the second and third columns in Fig. 6). Second, increased vertical transmission (larger values of p) is destabilizing because it tends to replace stable endemic equilibria by endemic cycles (compare the rows in Fig. 6). In the case of density-dependent demographics ($\lambda > 0$), increased vertical transmission also promotes disease invasion into a disease-free equilibrium.

4. Discussion

We have shown that one of the simplest SI epidemic models leads to sustained multi-generational oscillations when (i) the disease transmission period is temporally distinct from the reproduction period; (ii) virulence is such that infected individuals alone cannot survive; and (iii) disease transmission is density-dependent. These assumptions are well matched by host–pathogen systems where the host has discrete generations and its interaction with the pathogen is such that only certain age classes are susceptible to a highly virulent disease. This could apply to cyclic forest insects which are known to be infected by baculoviruses, which inflict high mortality only in larval stages of their hosts.

For example, western tent caterpillars (WTC, *Malacosoma californicum pluviale*) have one generation per year and overwinter as larvae. The larval stage can get infected by a baculovirus (nucleopolyhedrovirus, NPV). Both WTC abundance and NPV infection level show cyclic dynamics with a period of 8–11 years on Galiano Island, BC, Canada (Myers and Cory, 2013; 2016). A consistent characteristic of these cycles is reduced host fecundity in declining WTC populations, which is thought to be a sublethal effect of NPV infection (Rothman and Myers, 1996; Cory and Myers, 2009; Myers and Cory, 2016). Our model is thus based on some matching assumptions and shows qualitatively similar oscillations, even though it is neither tailored toward nor parameterized for this specific host–pathogen system.

The cycles in our model can be attributed to a *carry-over effect* (Royama, 1992; Ratikainen et al., 2008). Carry-over effects describe the situation when the fitness of an individual depends on how the individual did in the stages before. For example, the fertility of an individual in summer can depend on the availability of food during the winter, or the mortality in one season can depend on environmental contamination or injuries inflicted from fighting during another season. In our model, individual fitness (here in terms of fecundity) in the Reproduction period depends on what the individual experienced in the Infection period. If the individual gets infected, its fecundity will be reduced in the next period. The carry-over effect in our model is density-dependent, because the change in the infection status of an individual is determined by density-dependent disease transmission. Density-dependent carry-over effects give rise to delayed density-dependent population responses. While carry-over effects are defined at the individual level (considering the infection or physiological status of an individual), delayed density dependence is defined at the population level by considering how population growth is affected by population density in the previous generation. Importantly, both concepts can be destabilizing and cause higher-order cycles (Ratikainen et al., 2008).

The oscillations in our models are characterized by a phase shift with the disease prevalence lagging behind the total host population density (cf. Fig. 1). Moreover, the oscillations have long peri-

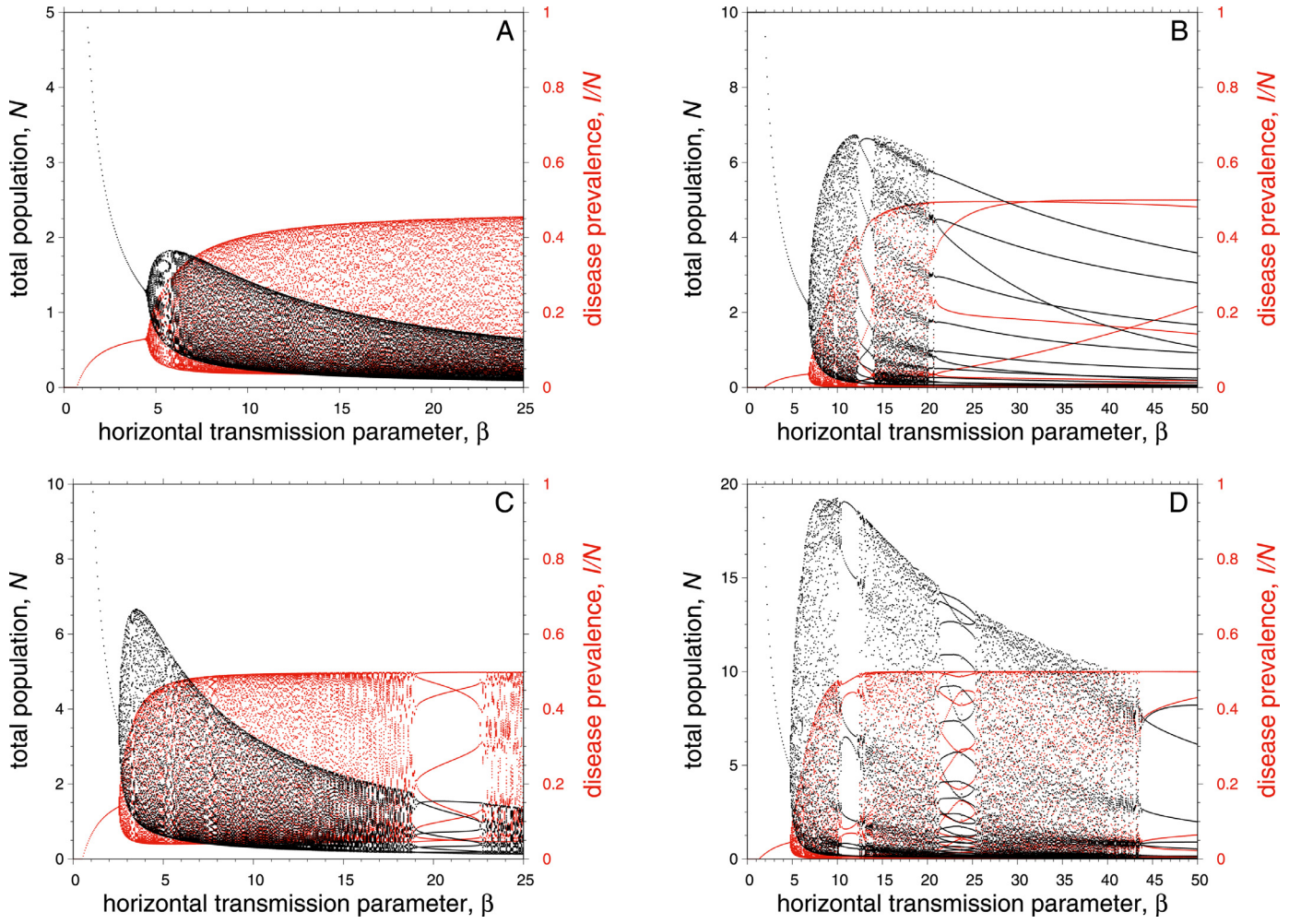

Fig. 4. Orbital bifurcation diagrams for varying transmission parameter β in model (4) with host density dependence. *Top*: $b_S = 2$, *bottom*: $b_S = 4$, *left*: $b_I = 0.5$, *right*: $b_I = 0.2$. For each value of β, the last 50 after 1,000 iterations are plotted. Initial conditions are drawn from pseudo-random uniform distribution in the unit square. Other parameters: $p = 0.5$, $\lambda = 0.1$. Note the different axes scales. (For interpretation of the references to color in this figure legend, the reader is referred to the web version of this article.)

ods that encompass several generations. As both reproduction and infection periods occur annually, the multi-annual cycles caused by their interplay clearly take place on another time scale stretching over more than one host generation. Observed periods of population cycles typically range from 3–5 years in voles and lemmings (Lambin et al., 2000), 4–6 years in red grouse (Hudson, 1992), and 8–15 years in forest-defoliating insects (Dwyer et al., 2004).

For cycles to occur in our model, the infection needs to suppress fecundity below a certain level. The critical level depends on the horizontal and vertical transmission parameters, the fecundity of susceptibles, and the strength of density dependence in reproduction (see Figs. 4 and 6). The fecundity of infected individuals needs to be at least below one for cycles to occur, which means that the infected part of the population has a negative growth rate. This is what causes the host population to decline after an outbreak with high infection prevalence.

A lot of work on cyclic species is based on food limitation, predation, and density-dependent mortality (Berryman, 2002). However, changes in reproduction, especially when carried over to the next generation, are also known to greatly influence population cycles (Münster-Swendsen, 1991; Kendall et al., 2005; Klemola et al., 2008; Inchausti and Ginzburg, 2009; Myers and Cory, 2013; Fauteux et al., 2015; Ginzburg and Krebs, 2015; Myers and Cory, 2016; Radchuk et al., 2016; Krebs et al., 2018; Myers, 2018). Previous mathematical models have already shown that disease-reduced reproduction can destabilize the host population and generate multi-year oscillations, but they all rest on additional assumptions like free-living infective stages (Anderson and May, 1980; 1981; Dobson and Hudson, 1992; White et al., 1996), exposed or latent classes (Anderson et al., 1981; Pugliese, 1991), seasonal forcing (Anderson and May, 1981; Brown, 1984; Smith et al., 2008), saturating incidences and highly nonlinear birth rates (Diekmann and Kretzschmar, 1991; Hochberg, 1991), and covert or sublethal infections (Boots and Norman, 2000; Boots et al., 2003).

It has been proven that continuous-time models of SI (and also SIS) type with density-dependent horizontal as well as vertical transmission, disease-reduced fecundity, disease-induced mortality, and density-dependent reproduction do not show sustained oscillations (Zhou and Hethcote, 1994). Hence, the novelty of our model is that multi-year oscillations can occur due to the temporally distinct periods of Infection and Reproduction. The latter are encapsulated by the order of events in the discrete-time formulation. By contrast, continuous-time models assume that all processes take place simultaneously, and they cannot produce cycles even when incorporating the same processes as in our model.

In a variation of our model with frequency-dependent rather than density-dependent transmission, we could not observe sustained oscillations (Hamelin et al., 2017). We suppose that density-dependent transmission, at least at small population densities, is needed for infection levels to decline at population troughs so

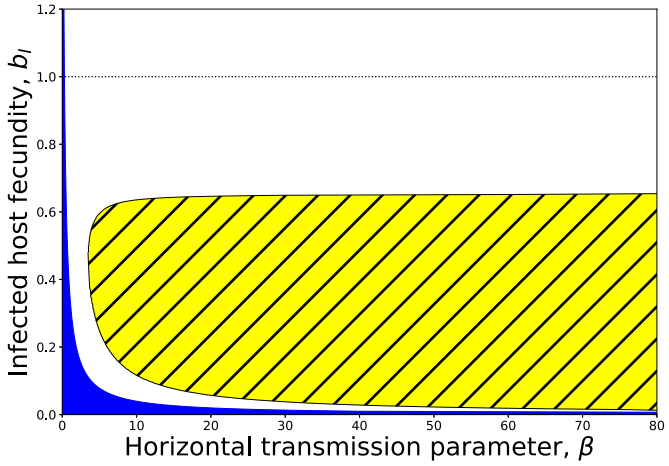

Fig. 5. Asymptotic behavior for varying horizontal transmission parameter β and infected host fecundity b_I in model (4) with host density dependence. The attractors are denoted by color: disease-free equilibrium (plain blue), stable coexistence equilibrium (plain white), endemic cycles (hatched yellow). The stability boundary between endemic cycles and the stable endemic equilibrium was found numerically for each value of b_I as the largest value for β allowing for significant convergence. Other parameter values: $b_S = 2$, $p = 0.5$, $\lambda = 0.1$. We remark that, depending on machine precision, there can be numerical artifacts for extremely large values of β (see Appendix E for more details). (For interpretation of the references to color in this figure legend, the reader is referred to the web version of this article.)

that the population can rebuild to start a new irruption. This is in line with SI type models where the host population exhibits a demographic Allee effect: with density-dependent transmission there can be limit cycles (Hilker et al., 2009), whereas with frequency-dependent transmission there are no sustained oscillations (Hilker et al., 2007).

To summarize, we have shown in this paper that a very simple discrete-time SI model can generate periodic or quasi-periodic multi-generational oscillations, both with density-dependent or density-independent host reproduction. The cycles are caused by virulence effects that are carried over from the infection season to the reproductive season. Our results underline the importance of sequentially occurring events in the course of a year, because the temporal separation between infection and virulence-affected reproduction can drive cycles that are impossible in continuous-time models where all processes take place simultaneously.

Any model makes limiting assumptions. Our discrete-time SI model based on the Poisson distribution assumes that the mean number of infectious contacts per susceptible host during the Infection period is proportional to the density of infected individuals at the beginning of that period. This means that newly infected individuals do not contribute to the epidemiological dynamics during the Infection period. This assumption fits a number of biological systems such as mono-cyclic diseases in plants (Madden et al., 2007), any situation in which the latent period is greater than the Infection period (e.g. rabies in foxes Anderson, 1982), or insect infections with latent baculoviruses (Cory and Myers, 2003; Il'inykh, 2007). Furthermore, by focusing on semelparous species (which die after the Reproduction period) we disregard the possible effects of disease-induced mortality. Since disease-reduced fecundity and disease-induced mortality are both expressions of virulence, it would be interesting to investigate whether the critical level of disease-induced fertility reduction could be lower in the presence of disease-induced mortality.

To take into account ongoing infections as well as deaths of infected hosts, an alternative model framework would be to consider epidemiological dynamics in continuous time, leading to a semi-discrete model, as in Hamelin et al. (2016a) for example. Interestingly, complex dynamics (multi-year cycles and chaos) occur in a related semi-discrete model (Mailleret et al., 2012), although host demographics were tailored for agricultural systems; namely, host density at the beginning of the Infection period was assumed to be always the same regardless of epidemics in the previous sea-

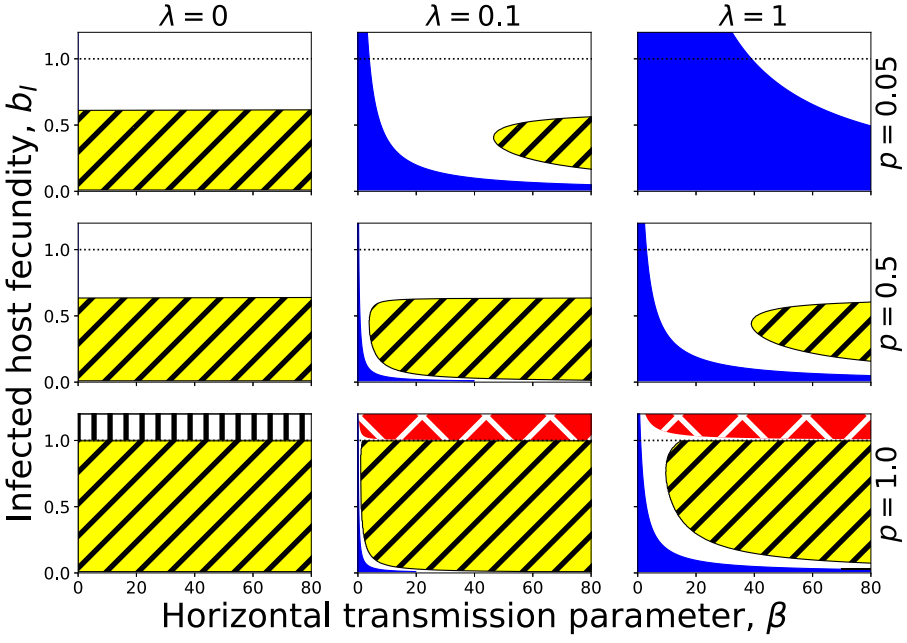

Fig. 6. Asymptotic behavior for varying horizontal transmission parameter β and infected host fecundity b_I in model (4) with host density dependence, for various vertical transmission parameters in rows: $p = 0.05$ (*top*), $p = 0.5$ (*middle*), and $p = 1$ (*bottom*), and various density dependence parameters in colums: $\lambda = 0$ (*left*), $\lambda = 0.1$ (*center*), $\lambda = 1$ (*right*). The panel in the middle corresponds to Fig. 5. The attractors are denoted by color: disease-free equilibrium (plain blue), stable coexistence equilibrium (plain white), endemic cycles (yellow with diagonal hatching), total-infection equilibrium (red with crossed hatching). For $\lambda = 0$ and sufficiently large b_I the infected population grows without bounds (vertical hatching). Other parameter value: $b_S = 2$. (For interpretation of the references to color in this figure legend, the reader is referred to the web version of this article.)

sons. Therefore, the mechanism driving the oscillations was not the same as the one described in this study. It would be interesting to extend the current approach to a semi-discrete model where host population dynamics follow a natural pattern. Preliminary investigations indicate that sustained oscillations are possible as well in a simple related semi-discrete model, but they do not depend on the parameters in the same way. Therefore, we leave this study for future research.

Acknowledgments

This work was partially conducted during the Multiscale Vectored Plant Viruses Working Group at the National Institute for Mathematical and Biological Synthesis, supported by the National Science Foundation through NSF Award #DBI-1300426, with additional support from The University of Tennessee, Knoxville. TAS has been supported by the Ministry of Science and Culture of Lower Saxony and by the Alexander von Humboldt Foundation.

Appendix A. Alternative order of events

Here, we assume that the period of Infection occurs after Reproduction:

$$t \underbrace{\rightarrow}_{\text{Reproduction}} t' \underbrace{\rightarrow}_{\text{Infection}} t+1.$$

The model takes the form:

$$\begin{aligned} S(t+1) &= S(t')\exp\left(-\beta I(t')\right),\\ I(t+1) &= I(t') + S(t')\left[1-\exp\left(-\beta I(t')\right)\right], \end{aligned} \tag{A.1}$$

where

$$\begin{aligned} S(t') &= \rho_S S(t) + \frac{b_S S(t) + (1-p) b_I I(t)}{1+\lambda[S(t)+I(t)]},\\ I(t') &= \rho_I I(t) + \frac{p b_I I(t)}{1+\lambda[S(t)+I(t)]}. \end{aligned} \tag{A.2}$$

For consistency with the model in the main text, we also assume $\rho_S = \rho_I = 0$ (semelparity) and, by combining (A.1) with (A.2), arrive at

$$\begin{aligned} S(t+1) &= \frac{b_S S(t) + (1-p) b_I I(t)}{1+\lambda N(t)} \exp\left(\frac{-\beta p b_I I(t)}{1+\lambda N(t)}\right),\\ I(t+1) &= \frac{I(t)\left[1-(1-p)b_I \exp\left(\frac{-\beta p b_I I(t)}{1+\lambda N(t)}\right)\right] + b_S S(t)\left[1-\exp\left(\frac{-\beta p b_I I(t)}{1+\lambda N(t)}\right)\right]}{1+\lambda N(t)}. \end{aligned} \tag{A.3}$$

Model (A.3) is structurally equivalent to model (4) in the main text. As the two models are permutations of the same two processes (Reproduction and Infection), they only differ in when the population densities are being censused (before Reproduction or before Infection). Hence, there are quantitative differences in the measured population densities, but the system dynamics of the two models are qualitatively the same (Åström et al., 1996; Hilker and Liz, 2013). We have checked this in numerical simulations and obtained the same bifurcation diagrams for model (A.3) as in Fig. 6. That is, both (A.3) and (4) show sustained multi-generational oscillations, so that our main results (Neimark–Sacker bifurcation and limit cycles) do not depend on the specific order of events (whether Reproduction precedes Infections or the other way around).

Appendix B. Historical aside: the deterministic Reed–Frost model

It seems that one of the first discrete-time epidemiological models is due to unpublished work by Reed and Frost from the 1920s, which is actually a rather classical model (see Wilson and Burke, 1942; Abbey, 1952; Sartwell, 1976; Daley and Gani, 1999; Allen, 2008). The deterministic version of the Reed–Frost model reads

$$S_{n+1} = S_n(1-p)^{I_n}, \quad I_{n+1} = S_n\left(1-(1-p)^{I_n}\right), \tag{B.1}$$

where p is the probability of "effective contact" (i.e., sufficient for disease transmission) between any two individuals of the host population during one time step. Note that this discrete-time SIR model has been communicated before the famous paper by Kermack and McKendrick (1927) was published. And note that it leads to the final size equation (Wilson and Burke, 1942), i.e. for $\alpha N > 1$, the system converges to some $N > S_\infty > 0$ and $I = 0$. Wilson and Burke (1942, p. 366) wrote "I strongly urged Dr. Frost to publish his theory of the epidemic curve, but he thought it too slight a contribution.", also quoted by Sartwell (1976). Yet, the Reed–Frost model implicitly assumes that both the latent and infectious periods are equal to one time step. This might explain why it is not so well known, despite its simplicity.

Letting $p = 1-\exp(-\beta)$, system (B.1) is equivalent to

$$S_{n+1} = S_n \exp(-\beta I_n), \quad I_{n+1} = S_n(1-\exp(-\beta I_n)).$$

This is almost the same model as the horizontal infection model given in (1), except that infected individuals do not survive between time steps. Our purely epidemic model (without host reproduction) in the Infection period can therefore be fairly credited to Reed and Frost.

Appendix C. Comparison with the Régnière (1984) model

We can rewrite model (4) as

$$\begin{aligned} S(t+1) &= (1-p)\left[\frac{b_I}{D_t} I(t) + \frac{b_I}{D_t}\Theta_t S(t)\right] + (1-P_t)\frac{b_S}{D_t} S(t),\\ I(t+1) &= p\left[\frac{b_I}{D_t} I(t) + \frac{b_I}{D_t}\Theta_t S(t)\right], \end{aligned} \tag{C.1}$$

where $D_t = 1+\lambda(S(t)+I(t))$ accounts for density-dependent demographics, $\Theta_t = 1-\exp(-\beta I(t))$ is the probability of infection over the course of the Infection period, and $b_I < 1 < b_S$. Régnière (1984) ignores density-dependent demographics, i.e. $D_t = 1$. In his model, the only nonlinear term is the probability of infection, for which he assumes

$$\hat{\Theta}_t = (1-\exp(-\beta I(t)))^{\psi}.$$

The additional parameter $\psi \geq 1$ accounts for larger spread of disease propagules. If we let $\psi = 1$, $D_t = 1$ ($\lambda = 0$), and the three parameters a, b, and c in the Régnière (1984) model be defined as follows:

$$a = b = b_I \quad \text{and} \quad c = b_S,$$

then the two models are equivalent. In Régnière (1984), parameters a, b, and c are the fecundity of "diseased", "newly infected", and disease-free hosts, respectively. With "diseased" individuals he refers to those who are born already being infected, i.e. vertically infected, whereas "newly infected" individuals are considered those who were born disease-free but got infected during the horizontal transmission period. That is, Régnière (1984) implicitly

tracks two different states of infection (getting infected either after horizontal or vertical transmission) and additional inter-seasonal effects (survival and fecundity depending on infection being acquired in the season with horizontal or vertical transmission). Also, note that the model in Régnière (1984) is derived by following a schematic diagram, where the order of events is not explicit and, therefore, some of the underlying assumptions remain concealed.

Régnière (1984) assumes $a < 1$ and $c > 1$, and $a \leq b < c$. The latter differs from our model where $a = b$. Furthermore, we consider $\psi = 1$ and $D_t \geq 1$ ($\lambda \geq 0$).

Appendix D. Equilibria and stability analysis

D1. Density-independent reproduction ($\lambda = 0$)

We consider model (4) with $\lambda = 0$ for $b_S > 1$, $b_I < b_S$ and $0 < p \leq 1$ (the case where $p = 0$ immediately drives the infected population to extinction and leaves the susceptible population to grow geometrically):

$$S(t+1) = (1-p)b_I[I(t)+S(t)] + [b_S - (1-p)b_I]S(t)\mathrm{e}^{-\beta I(t)}$$
$$I(t+1) = pb_I\left(I(t)+S(t)\left[1-\mathrm{e}^{-\beta I(t)}\right]\right).$$

The trivial point (0,0) is always an unstable equilibrium. It has the eigenvalues $b_S > 1$ and pb_I.

Due to geometric host population growth in the absence of disease, the trivial equilibrium is the only equilibrium with $S^* = 0$ or $I^* = 0$. In particular, there is no disease-free or total-infection equilibrium. However, when having full vertical transmission $p = 1$, there is a possibility for a totally-infected population with $b_I > 1$ to grow geometrically in the absence of susceptibles; this is similar to the geometric host population growth in the absence of disease.

In the general case, all non-trivial equilibria must satisfy the two following conditions:

$$1 - b_I = (b_S - b_I)\frac{S^*}{S^*+I^*}\mathrm{e}^{-\beta I^*} \quad \text{and} \quad \frac{S^*}{I^*} = \frac{b_S - b_I}{(b_S-1)pb_I} - 1 =: R(b_S, b_I, p).$$

The first condition imposes that $b_I < 1$. If this is the case, then $R(b_S, b_I, p)$ is positive. Moreover, there can be at most one coexistence equilibrium since, if it exists, it must have the components:

$$S^* = R(b_S, b_I, p)\frac{L(b_S, b_I, p)}{\beta}, \quad I^* = \frac{L(b_S, b_I, p)}{\beta}, \tag{D.1}$$

with

$$L(b_S, b_I, p) = \ln\left(\frac{b_S - b_I - (b_S-1)pb_I}{1-b_I}\right).$$

The assumption that $b_I < 1$ is sufficient for both $R(b_S, b_I, p)$ and $L(b_S, b_I, p)$ to be defined and positive. As a consequence, it is the only condition for the existence of the coexistence equilibrium, which is unique.

The Jacobian matrix evaluated at the coexistence equilibrium can be written as:

$$\begin{pmatrix} 1 - \frac{(b_S-1)p(1-p)b_I^2}{b_S-b_I-(b_S-1)pb_I} & (1-p)b_I + \frac{b_S-(1-p)b_I}{pb_I}L(b_S,b_I,p)\frac{b_I-1}{b_S-1} \\ pb_I\frac{b_S-1-(b_S-1)pb_I}{b_S-b_I-(b_S-1)pb_I} & pb_I\left[1+\frac{1-b_I}{(b_S-1)pb_I}L(b_S,b_I,p)\right] \end{pmatrix}.$$

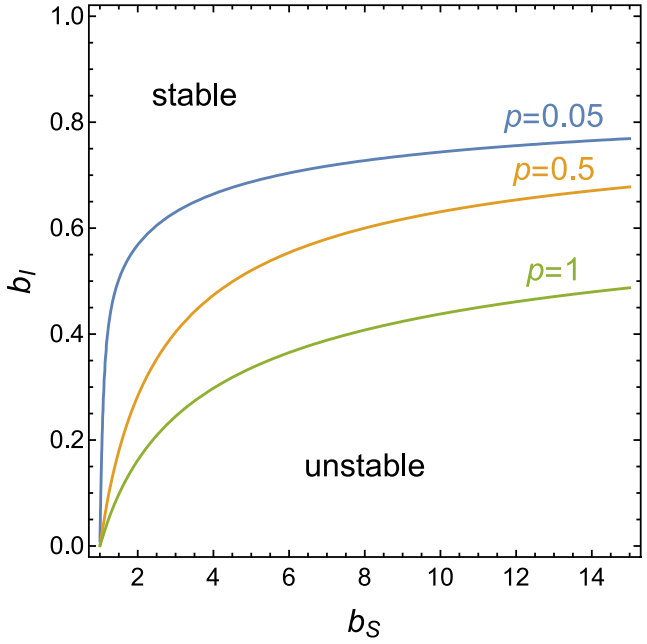

Fig. D.1. Stability diagram for the endemic coexistence equilibrium in the model with density-independent reproduction ($\lambda = 0$). The stability boundary is obtained from the Jury conditions and shown for different values for the vertical transmission parameter. The endemic coexistence equilibrium is locally asymptotically stable above and unstable below the boundaries.

Thus, the stability of the coexistence equilibrium does not depend on the horizontal transmission parameter β. But β does affect the population densities at equilibrium: the larger β, the smaller S^* and the smaller I^* (see Eq. (D.1)).

To analyze the stability of the coexistence equilibrium, we now employ the Jury conditions (e.g. Allen, 2007, pp. 64). Let

$$A = 1 - \det J,$$
$$B = \det J - \mathrm{Tr}\, J + 1,$$
$$C = \det J + \mathrm{Tr}\, J + 1.$$

The Jury conditions $A, B, C > 0$ are necessary and sufficient conditions for the equilibrium to be locally asymptotically stable. We have

$$B = -(1-b_I)\log\left(\frac{1-b_I}{b_S - b_I - pb_I(b_S-1)}\right) > 0.$$

Also,

$$C = \frac{(1+b_S)[b_S - b_I - pb_I(b_S-1)]B + 2(b_S-1)[b_S(1-pb_I^2) - b_I(1-p)]}{(b_S-1)[b_S - b_I - pb_I(b_S-1)]}.$$

Numerical explorations suggest $C > 0$, so that the stability of the coexistence equilibrium entirely depends on the sign of

$$A = 1 + \frac{(1-b_I)b_S\left([b_S - b_I - pb_I(b_S-1)]\log\left(\frac{1-b_I}{b_S-b_I-pb_I(b_S-1)}\right) - pb_I(b_S-1)\right)}{(b_S-1)[b_S - b_I - pb_I(b_S-1)]}.$$

The stability of the coexistence equilibrium is therefore determined by three parameters. Fig. D.1 shows a stability diagram in the (b_S, b_I) parameter plane for different values of p. The coexistence equilibrium gets destabilized by high reproductive capability (large b_S), high virulence (low b_I), and imperfect vertical transmission (low p).

Recall that, in the absence of infection, the host population grows geometrically in the density-independent model. We have shown that the disease may regulate the unbounded host growth to a stable endemic equilibrium (in the analysis above) or to sustained endemic oscillations (shown numerically in the main text).

D2. Density-dependent reproduction ($\lambda > 0$)

We consider model (4) with $\lambda > 0$, again for $b_S > 1$, $b_I < b_S$ and $0 < p \leq 1$. There are four potential equilibria.

1. The trivial extinction equilibrium (0,0) always exists. The eigenvalues of the Jacobian matrix evaluated at this trivial equilibrium are b_S and pb_I; since $b_S > 1$, this equilibrium is unstable. The eigenvalues are the same as for the density-independent model; this is because density dependence does not play a role at the trivial equilibrium.
2. The disease-free equilibrium $\left(\frac{b_S-1}{\lambda}, 0\right)$ exists when there is density dependence ($\lambda > 0$). It is stable if
$$\beta \leq \frac{\lambda(b_S - pb_I)}{pb_I(b_S - 1)}.$$
3. The total-infection equilibrium is $(0, \frac{b_I-1}{\lambda})$. The conditions for its existence are: density dependence ($\lambda > 0$), perfect vertical transmission ($p = 1$), and sustainability of an infected population ($b_I > 1$). It is stable if
$$\beta \geq \frac{\lambda}{b_I - 1} \ln\left(\frac{b_S}{b_I}\right).$$
4. There can be a coexistence equilibrium (S^*, I^*). The Jacobian matrix evaluated at any equilibrium can be written as:
$$\begin{pmatrix} \frac{qb_I+(b_S-qb_I)e^{-\beta I^*}(1+\lambda I^*)}{(1+\lambda N^*)^2} & \frac{qb_I-(b_S-qb_I)S^*e^{-\beta I^*}(\beta+\lambda+\beta\lambda N^*)}{(1+\lambda N^*)^2} \\ pb_I\frac{1-e^{-\beta I^*}(1+\lambda I^*)}{(1+\lambda N^*)^2} & pb_I\frac{1+S^*e^{-\beta I^*}(\beta+\lambda+\beta\lambda N^*)}{(1+\lambda N^*)^2} \end{pmatrix},$$
where $N^* = S^* + I^*$ and $q = 1 - p$. Numerical simulations in the main text reveal that the coexistence equilibrium can be stable or unstable. The bifurcation diagrams in Fig. 4 suggest that the change in stability is brought about by a Neimark–Sacker bifurcation.

Appendix E. Numerical warning

For certain extreme parameter values, we have observed numerical artifacts when iterating model (4) numerically. They are due to numerical inaccuracies when very small numbers are approximated as zero in simulations. These artifacts occur when the coexistence equilibrium is unstable and when there are limit cycle oscillations on an invariant curve. For rather large values of the transmission parameter β, the invariant curve gets very close to the axes of the phase plane and suddenly the oscillations "collapse" in the simulations. In that case, numerical simulations approached the disease-free equilibrium, for any simulation length we considered. The surprising result is that the disease-free equilibrium is an unstable saddle point for those parameter values, which is why orbits should leave the vicinity of the disease-free equilibrium sooner or later. The resolution is that the number of the infected population density gets so small that it is approximated numerically as zero such that the simulation gets trapped on the boundary axis determined by $I_t = 0$. A similar numerical artifact has been observed by Kang and Armbruster (2011) in a discrete-time plant–herbivore model.

This artifact is a numerical problem. In practice, we could have extinction due to stochastic effects already for smaller values of β—namely when the invariant curve gets just close enough to one of the axes. Actually, this could apply not only to I_t but also to S_t.

References

Abbey, H., 1952. An examination of the Reed-Frost theory of epidemics. Hum. Biol. 24, 201–233.

Allen, L.J.S., 2007. An Introduction to Mathematical Biology. Pearson Prentice Hall, Upper Saddle River NJ.

Allen, L.J.S., 2008. An introduction to stochastic epidemic models. In: Brauer, F., van den Driessche, P., Wu, J. (Eds.), Mathematical Epidemiology. Springer, Berlin, pp. 81–130.

Altizer, S., Bartel, R., Han, B.A., 2011. Animal migration and infectious disease risk. Science 331, 296–302.

Altizer, S., Hochachka, W.M., Dhondt, A.A., 2004. Seasonal dynamics of mycoplasmal conjunctivitis in eastern North American house finches. J. Anim. Ecol. 73, 309–322.

Altizer, S., Hosseini, A.D.P., Hudson, P., Pascual, M., Rohani, P., 2006. Seasonality and the dynamics of infectious diseases. Ecol. Lett. 9, 467–484.

Anderson, R.M., 1982. Fox rabies. In: Anderson, R.M. (Ed.), The Population Dynamics of Infectious Diseases: Theory and Applications. Springer, Dordrecht, pp. 242–261.

Anderson, R.M., Jackson, H.C., May, R.M., Smith, A.M., 1981. Population dynamics of fox rabies in Europe. Nature 289, 765–770.

Anderson, R.M., May, R.M., 1980. Infectious diseases and population cycles of forest insects. Science 210, 658–661.

Anderson, R.M., May, R.M., 1981. The population dynamics of microparasites and their invertebrate hosts. Philos. Trans. R. Soc. Lond. B 291, 451–524.

Åström, M., Lundberg, P., Lundberg, S., 1996. Population dynamics with sequential density-dependencies. Oikos 75, 174–181.

Begon, M., Bennett, M., Bowers, R.G., French, N.P., Hazel, S.M., Turner, J., 2002. A clarification of transmission terms in host-microparasite models: numbers, densities and areas. Epidemiol. Infect. 129, 147–153.

van den Berg, F., Bacaer, N., Metz, J.A., Lannou, C., van den Bosch, F., 2011. Periodic host absence can select for higher or lower parasite transmission rates. Evol. Ecol. 25 (1), 121–137.

Berryman, A.A. (Ed.), 2002. Population Cycles: The Case for Trophic Interactions. Oxford University Press, New York.

Beverton, R.J.H., Holt, S.J., 1957. On the Dynamics of Exploited Fish Populations. Fishery Investigations, II. Ministry of Agriculture, Fisheries and Food.

Bolzoni, L., Dobson, A.P., Gatto, M., De Leo, G.A., 2008. Allometric scaling and seasonality in the epidemics of wildlife diseases. Am. Nat. 172, 818–828.

Boots, M., Greenman, J., Ross, D., Norman, R., Hails, R., Sait, S., 2003. The population dynamical implications of covert infections in host–microparasite interactions. J. Anim. Ecol. 72, 1064–1072.

Boots, M., Norman, R., 2000. Sublethal infection and the population dynamics of host–microparasite interactions. J. Anim. Ecol. 69, 517–524.

Briggs, C.J., Godfray, H.C.J., 1995. The dynamics of insect-pathogen interactions in stage-structured populations. Am. Nat. 145, 855–887.

Briggs, C.J., Godfray, H.C.J., 1995. Models of intermediate complexity in insect–pathogen interactions: population dynamics of the microsporidian pathogen, Nosema pyrausta, of the European corn borer, Ostrinia nubilalis. Parasitology 111, S71–S89.

Briggs, C.J., Godfray, H.C.J., 1996. The dynamics of insect–pathogen interactions in seasonal environments. Theor. Popul. Biol. 50, 149–177.

Brown, G.C., 1984. Stability in an insect-pathogen model incorporating age-dependent immunity and seasonal host reproduction. Bull. Math. Biol. 46, 139–153.

Cory, J.S., Myers, J.H., 2003. The ecology and evolution of insect baculoviruses. Annu. Rev. Ecol. Evol. Syst. 34, 239–272.

Cory, J.S., Myers, J.H., 2009. Within and between population variation in disease resistance in cyclic populations of western tent caterpillars: a test of the disease defence hypothesis. J. Anim. Ecol. 78, 646–655.

Daley, D.J., Gani, J., 1999. Epidemic Modelling: An Introduction. Cambridge University Press, Cambridge, UK.

de Witt, C.T., 1960. On Competition. Versl. Landbouwk. Onderz.

Desprez-Loustau, M.-L., Hamelin, F.M., Marçais, B., 2019. The ecological and evolutionary trajectory of oak powdery mildew in Europe. In: Wilson, K., Fenton, A., Tompkins, D. (Eds.), Wildlife Disease Ecology: Linking Theory to Data and Application. Cambridge University Press, Cambridge, pp. 429–457.

Diekmann, O., Kretzschmar, M., 1991. Patterns in the effects of infectious diseases on population growth. J. Math. Biol. 29, 539–570.

Dingle, H., 1996. Migration: The Biology of Life on the Move. Oxford University Press, New York.

Dobson, A.P., Hudson, P.J., 1992. Regulation and stability of a free-living host-parasite system: Trichostrongylus tenuis in red grouse. II. Population models. J. Anim. Ecol. 61, 487–498.

Dwyer, G., Dushoff, J., Yee, S.H., 2004. The combined effects of pathogens and predators on insect outbreaks. Nature 430, 341–345.

Fauteux, D., Gauthier, G., Berteaux, D., 2015. Seasonal demography of a cyclic lemming population in the Canadian Arctic. J. Anim. Ecol. 84, 1412–1422.

Folstad, I., Nilssen, A.C., Halvorsen, O., Andersen, J., 1991. Parasite avoidance: the cause of post-calving migrations in Rangifer? Can. J. Zool. 69, 2423–2429.

Ginzburg, L.R., Krebs, C.J., 2015. Mammalian cycles: internally defined periods and interaction-driven amplitudes. PeerJ 3, e1180.

Hamelin, F.M., Allen, L.J.S., Prendeville, H.R., Hajimorad, M.R., Jeger, M.J., 2016a. The evolution of plant virus transmission pathways. J. Theor. Biol. 396, 75–89.

Hamelin, F.M., Bisson, A., Desprez-Loustau, M.-L., Fabre, F., Mailleret, L., 2016b. Temporal niche differentiation of parasites sharing the same plant host: oak powdery mildew as a case study. Ecosphere 7, e01517.

Hamelin, F.M., Castel, M., Poggi, S., Andrivon, D., Mailleret, L., 2011. Seasonality and the evolutionary divergence of plant parasites. Ecology 92, 2159–2166.

Hamelin, F.M., Hilker, F.M., Sun, T.A., Jeger, M.J., Hajimorad, M.R., Allen, L.J.S., Pren-

deville, H.R., 2017. The evolution of parasitic and mutualistic plant–virus symbioses through transmission-virulence trade-offs. Virus Res. 241, 77–87.
Hilker, F.M., Allen, L.J.S., Bokil, V.A., Briggs, C.J., Feng, Z., Garrett, K.A., Gross, L.J., Hamelin, F.M., Jeger, M.J., Manore, C.A., Power, A.G., Redinbaugh, M.G., Rúa, M.A., Cunniffe, N.J., 2017. Modeling virus coinfection to inform management of maize lethal necrosis in Kenya. Phytopathology 107, 1095–1108.
Hilker, F.M., Langlais, M., Malchow, H., 2009. The Allee effect and infectious diseases: extinction, multistability, and the (dis-)appearance of oscillations. Am. Nat. 173, 72–88.
Hilker, F.M., Langlais, M., Petrovskii, S.V., Malchow, H., 2007. A diffusive SI model with Allee effect and application to FIV. Math. Biosci. 206, 61–80.
Hilker, F.M., Liz, E., 2013. Harvesting, census timing and "hidden" hydra effects. Ecol. Complex. 14, 95–107.
Hinshaw, V.S., Webster, R.G., Turner, B., 1980. The perpetuation of orthomyxoviruses and paramyxoviruses in Canadian waterfowl. Can. J. Microbiol. 26, 622–629.
Hochberg, M.E., 1991. Non-linear transmission rates and the dynamics of infectious disease. J. Theor. Biol. 153, 301–321.
Hosseini, P.R., Dhondt, A.A., Dobson, A., 2004. Seasonality and wildlife disease: how seasonal birth, aggregation and variation in immunity affect the dynamics of Mycoplasma gallisepticum in house finches. Proc. R. Soc. Lond. B 271, 2569–2577.
Hoye, B.J., Munster, V.J., Nishiura, H., Fouchier, R.A.M., Madsen, J., Klaassen, M., 2011. Reconstructing an annual cycle of interaction: natural infection and antibody dynamics to avian influenza along a migratory flyway. Oikos 120, 748–755.
Hudson, P.J., 1992. Grouse in Space and Time: The Population Ecology of a Managed Gamebird. Game Conservancy Ltd., Hampshire, UK.
Il'inykh, A.V., 2007. Epizootiology of baculoviruses. Biol. Bull. 34, 434–441.
Inchausti, P., Ginzburg, L.R., 2009. Maternal effects mechanism of population cycling: a formidable competitor to the traditional predator–prey view. Philos. Trans. R. Soc. B 364, 1117–1124.
Kang, Y., Armbruster, D., 2011. Noise and seasonal effects on the dynamics of plant–herbivore models with monotonic plant growth functions. Int. J. Biomath. 4, 255–274.
Keeling, M.J., Rohani, P., 2007. Modeling Infectious Diseases in Humans and Animals. Princeton University Press, Princeton.
Kendall, B.E., Ellner, S.P., McCauley, E., Wood, S.N., Briggs, C.J., Murdoch, W.W., Turchin, P., 2005. Population cycles in the pine looper moth: dynamical tests of mechanistic hypotheses. Ecol. Monogr. 75, 259–276.
Kermack, W.O., McKendrick, A.G., 1927. Contributions to the mathematical theory of epidemics – I. Proc. R. Soc. Lond. A 115, 700–721.
Klemola, T., Andersson, T., Ruohomäki, K., 2008. Fecundity of the autumnal moth depends on pooled geometrid abundance without a time lag: implications for cyclic population dynamics. J. Anim. Ecol. 77, 597–604.
Krauss, S., Walker, D., Pryor, S.P., Niles, L., Chenghong, L., Hinshaw, V.S., Webster, R.G., 2004. Influenza A viruses of migrating wild aquatic birds in North America. Vector-Borne Zoonotic Dis. 4, 177–189.
Krebs, C.J., Boonstra, R., Boutin, S., 2018. Using experimentation to understand the 10-year snowshoe hare cycle in the boreal forest of North America. J. Anim. Ecol. 87, 87–100.
Lambin, X., Petty, S.J., Mackinnon, J.L., 2000. Cyclic dynamics in field vole populations and generalist predation. J. Anim. Ecol. 69, 106–119.
Loehle, C., 1995. Social barriers to pathogen transmission in wild animal populations. Ecology 76, 326–335.
Madden, L.V., Hughes, G., Van Den Bosch, F., 2007. The study of plant disease epidemics. American Phytopathology Society.
Mailleret, L., Castel, M., Montarry, J., Hamelin, F.M., 2012. From elaborate to compact seasonal plant epidemic models and back: is competitive exclusion in the details? Theor. Ecol. 5, 311–324.
Mailleret, L., Lemesle, V., 2009. A note on semi-discrete modelling. Philos. Trans. R. Soc. Lond. A 367, 4779–4799.
Miller, L.K. (Ed.), 2013. The Baculoviruses. Springer, New York.
Munster, V.J., Baas, C., Lexmond, P., Waldenström, J., Wallensten, A., Fransson, T., Rimmelzwaan, G.F., Beyer, W.E.P., Schutten, M., Olsen, B., Osterhaus, A.D.M.E., Fouchier, R.A.M., 2007. Spatial, temporal, and species variation in prevalence of influenza A viruses in wild migratory birds. PLoS Pathog. 3, e61.
Münster-Swendsen, M., 1991. The effect of sublethal neogregarine infections in the spruce needleminer, Epinotia tedella (Lepidoptera: Tortricidae). Ecol. Entomol. 16, 211–219.
Myers, J.H., 2018. Population cycles: generalities, exceptions and remaining mysteries. Proc. R. Soc. Lond. B 285, 20172841.
Myers, J.H., Cory, J.S., 2013. Population cycles in forest lepidoptera revisited. Annu. Rev. Ecol. Evol. Syst. 44, 565–592.
Myers, J.H., Cory, J.S., 2016. Ecology and evolution of pathogens in natural populations of Lepidoptera. Evol. Appl. 9, 231–247.
Norris, D.R., 2005. Carry-over effects and habitat quality in migratory populations. Oikos 109, 178–186.
Pastoret, P.P., Brochier, B., 1999. Epidemiology and control of fox rabies in Europe. Vaccine 17, 1750–1754.
Pugliese, A., 1991. An S → E → I epidemic model with varying total population size. In: Busenberg, S.N., Martelli, M. (Eds.), Differential Equation Models in Biology, Epidemiology and Ecology. Springer, Berlin, pp. 121–138.
Radchuk, V., Ims, R.A., Andreassen, H.P., 2016. From individuals to population cycles: the role of extrinsic and intrinsic factors in rodent populations. Ecology 97, 720–732.
Ratikainen, I.I., Gill, J.A., Gunnarsson, T.G., Sutherland, W.J., Kokko, H., 2008. When density dependence is not instantaneous: theoretical developments and management implications. Ecol. Lett. 11, 184–198.
Régnière, J., 1984. Vertical transmission of diseases and population dynamics of insects with discrete generations: a model. J. Theor. Biol. 107, 287–301.
Rothman, L.D., Myers, J.H., 1996. Debilitating effects of viral diseases on host Lepidoptera. J. Invertebr. Pathol. 67, 1–10.
Royama, T., 1992. Analytical Population Dynamics. Chapman & Hall, London.
Sartwell, P.E., 1976. Memoir on the reed-frost epidemic theory. Am. J. Epidemiol. 100, 138–140.
Smith, M.J., White, A., Sherratt, J.A., Telfer, S., Begon, M., Lambin, X., 2008. Disease effects on reproduction can cause population cycles in seasonal environments. J. Anim. Ecol. 77, 378–389.
Turchin, P., 2003. Complex Population Dynamics. A Theoretical/Empirical Synthesis. Princeton University Press, Princeton NJ.
Volkman, L.E., 1997. Nucleopolyhedrovirus interactions with their insect hosts. Adv. Virus Res. 48, 313–348.
White, A., Bowers, R.G., Begon, M., 1996. Host-pathogen cycles in self-regulated forest insect systems: resolving conflicting predictions. Am. Nat. 148, 220–225.
Wilson, E.B., Burke, M.H., 1942. The epidemic curve. Proc. Natl. Acad. Sci. 28, 361–367.
Zhou, J., Hethcote, H.W., 1994. Population size dependent incidence in models for diseases without immunity. J. Math. Biol. 32, 809–834.